JACS
JOURNAL OF THE AMERICAN CHEMICAL SOCIETY
pubs.acs.org/JACS
Article

Light-Powered Dissipative Assembly of Diazocine Coordination Cages

Haeri Lee, Jacopo Tessarolo, Daniel Langbehn, Ananya Baksi, Rainer Herges, and Guido H. Clever*

Cite This: J. Am. Chem. Soc. 2022, 144, 3099−3105
Read Online
ACCESS | Metrics & More | Article Recommendations | Supporting Information

ABSTRACT: Stimuli-responsive coordination cages allow reversible control over guest binding and release, relevant for adaptive receptors, carriers, catalysts, and complex systems. Light serves as an advantageous stimulus, as it can be applied with precise spatial and temporal resolution without producing chemical waste products. We report the first Pd-mediated coordination cage based on ligands embedding a diazocine photoswitch. While the thermodynamically more stable *cis*-photoisomer sloppily assembles to a mixture of species with general formula $[Pd_n$***cis***-$L_{2n}]$, the less stable *trans*-isomer yields a defined $[Pd_2$***trans***-$L_4]$ cage that reversibly converts back to the *cis*-system by irradiation at 530 nm or thermal relaxation. The $[Pd_n$***cis***-$L_{2n}]$ species do not bind a given guest; however, $[Pd_2$***trans***-$L_4]$ is able to encapsulate a bis-sulfonate as long as it is kept assembled, requiring continuous irradiation at 385 nm. In the absence of UV light, thermal relaxation results in back-switching and guest release. Assembly and properties of the system were characterized by a combination of NMR, ion mobility ESI-MS, single-crystal X-ray diffraction, and UV−vis absorption studies.

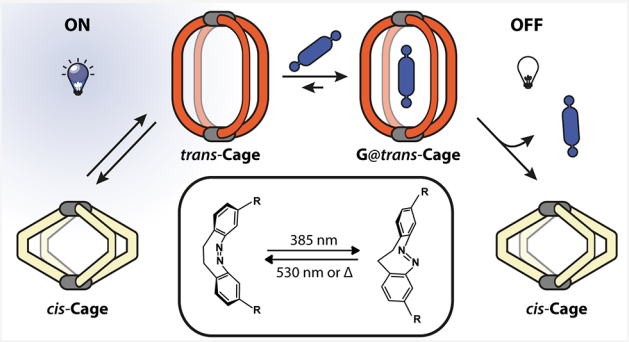

INTRODUCTION

The coordination-driven assembly of functional building blocks into supramolecular structures allows creating advanced nanosystems such as allosteric receptors, regulated catalysts, molecular machines, and stimuli-responsive materials. In many cases, the function of such systems requires nanosized cavities able to host guest molecules.[1−4] Response to external stimuli can then be employed to trigger structural rearrangements, affecting the host−guest binding affinity, thus establishing control over guest uptake and release.[5−12] Among various stimuli (e.g., pH,[13−15] temperature,[16] solvent,[17] electrochemical,[18,19] or chemical input[20,21]), light is a highly advantageous reagent, as it can be precisely administered with temporal and spatial resolution, is available from cheap LED sources, and is essentially waste-free. The light-triggered modification of structure and function of (supra)molecular systems can be achieved using dedicated photoswitches such as azobenzenes,[22,23] dithienylethenes,[24,25] other hindered alkenes,[26,27] indigoids,[28] and spiropiranes,[29,30] just to name a few. At the same time, light can be used as a fuel to drive systems away from thermal equilibrium, generating dissipative self-assembled systems.[31,32]

Although the commonly known photoswitches have been studied intensively before, reports on their implementation into discrete metallosupramolecular self-assemblies, especially as an integral part of the ligand backbone, remain rather scarce. For example, Wezenberg and Feringa incorporated their overcrowded alkene motor to trigger structural reorganization in Pd_2L_4 cages,[33] Liu and co-workers reported a Pd_2L_4 species that undergoes disassembly/reassembly upon isomerization of azobenzene moieties,[34] while the group of Hardie exploited the same photochromic unit to report a structural switch in an Ir_3L_2 assembly.[35] Besides these examples, the so far most intensely studied photoswitchable unit in ligand backbones is the dithienylethene (DTE) moiety. Our group previously reported a series of systems based on Pd^{II} cations and DTE ligands to control structural rearrangements and to tune guest selectivity, uptake, and release in a fully reversible fashion in homo- and heteroleptic cages.[8,10,36,37] Similar systems have been applied to control the topology of supramolecular gels[38] and to tune the emission properties of Eu_2L_4 helicates[39] or have been implemented in Pt-based metallacycles to trigger structural rearrangements or photochromic properties.[25,40]

Recently a new class of azo group-based photoswitches, namely, diazocines, has emerged as promising candidates for creating molecular switches and stimuli-responsive materials.[41,42] At first glance, the bridged diazocines seem similar to the archetypical azobenzenes; however, they are thermody-

Received: November 14, 2021
Published: January 26, 2022

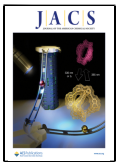

https://doi.org/10.1021/jacs.1c12011
J. Am. Chem. Soc. 2022, 144, 3099−3105

namically most stable in their *cis*-isomeric form. The metastable *trans*-isomer is formed upon irradiation at 385 nm, possessing a thermal lifetime of a few hours at room temperature. As compared to azobenzenes, diazocines are more rigid with a smaller number of conformational degrees of freedom and therefore allow a more controlled photochemically induced movement.[43] Herein, we report the implementation of a diazocine moiety into the backbone of a banana-shaped bis-pyridyl ligand under full preservation of its photoswitching properties. Self-assembly with Pd^{II} cations leads to the formation of Pd_nL_{2n} supramolecular assemblies. Interestingly, when the diazocine is used in the stable *cis*-isomeric form, structural strain seems to hamper formation of a defined structure as exclusive product. The diazocine in the metastable *trans*-isomeric form, however, neatly assembles to lantern-shaped cage $[Pd_2(\textbf{\textit{trans}-L})_4]$ as a single species. Formation of this species by metallosupramolecular assembly seems energetically favored compared to the *cis*-analogue, but it exists only as a transient assembly, whose population has to be kept up by continuous irradiation with UV light. Interestingly, the $[Pd_2(\textbf{\textit{trans}-L})_4]$ species is able to host a bis-sulfonate guest, while the structural change to the *cis*-analogue leads to guest release. Hence, the system resides in a state dominated by the prevalence of the $[\mathbf{G}@Pd_2\textbf{\textit{trans}-L}_4]$ host–guest complex via a dissipative self-assembly process, only as long as it is powered with light of 385 nm wavelength. Removal of the stimulus leads to thermal relaxation of the backbone, formation of $[Pd_n\textbf{\textit{cis}-L}_{2n}]$, and guest release.

RESULTS AND DISCUSSION

Photoswitchable bis-pyridyl ligand (Z)-3,8-bis(pyridin-3-ylethynyl)-11,12-dihydrodibenzo[*c*,*g*]-[1,2]diazocine (**L**) was synthesized by Sonogashira coupling between (*Z*)-3,8-diiodo-11,12-dihydrodibenzo[*c*,*g*][1,2]diazocine[42] and 3-ethynylpyridine (Supporting Information). The ligand forms as a thermodynamically stable *cis*-isomer (***cis*-L**). Irradiation at 385 nm rapidly generates the *trans*-isomer (***trans*-L**), while irradiation at 530 nm or thermal relaxation reverses the process (Figure 1a). The photochemical properties were investigated by ^{1}H NMR and UV–vis absorption spectroscopies (Figure 1b–d). Upon irradiation of a dimethylformamide (DMF) or acetonitrile solution of ***cis*-L**, a new set of signals appeared in the NMR spectrum (Figure 1b$_{i,ii}$), assigned to formation of ***trans*-L**. The conversion is not quantitative, and the photostationary state (PSS) was determined as a 62% *trans*/*cis*-form ratio by NMR signal integration. The coexistence of the two isomers is confirmed also by DOSY measurements, where the two species have clearly distinguishable diffusion coefficients measured as $D_{\textit{cis}\text{-L}} = 4.35 \times 10^{-10}$ and $D_{\textit{trans}\text{-L}} = 6.22 \times 10^{-10}$ (Figure 1b$_{iii}$). Thermal relaxation from ***trans*-L** to ***cis*-L** was monitored by ^{1}H NMR, resulting in a half-lifetime of 7.2 h at 298 K (Figure 1d). The thermal relaxation process (or irradiation with 530 nm) results also in a color change, from red to pale yellow in solution. In the UV–vis spectrum, ***cis*-L** is characterized by an absorption maximum at 399 nm (Figure 1c). Upon irradiation with a 385 nm LED, a new absorption band at 483 nm appears, characteristic for ***trans*-L** (Figure 1c). Upon irradiation with a 530 nm LED, the *cis*-isomer is fully restored within 5 min. Thermal back-switching of metastable ***trans*-L** was investigated also with absorption spectroscopy (Figure 1c, SI), and rate constants at different temperatures were used to calculate the activation parameters for the process (Figure S33).

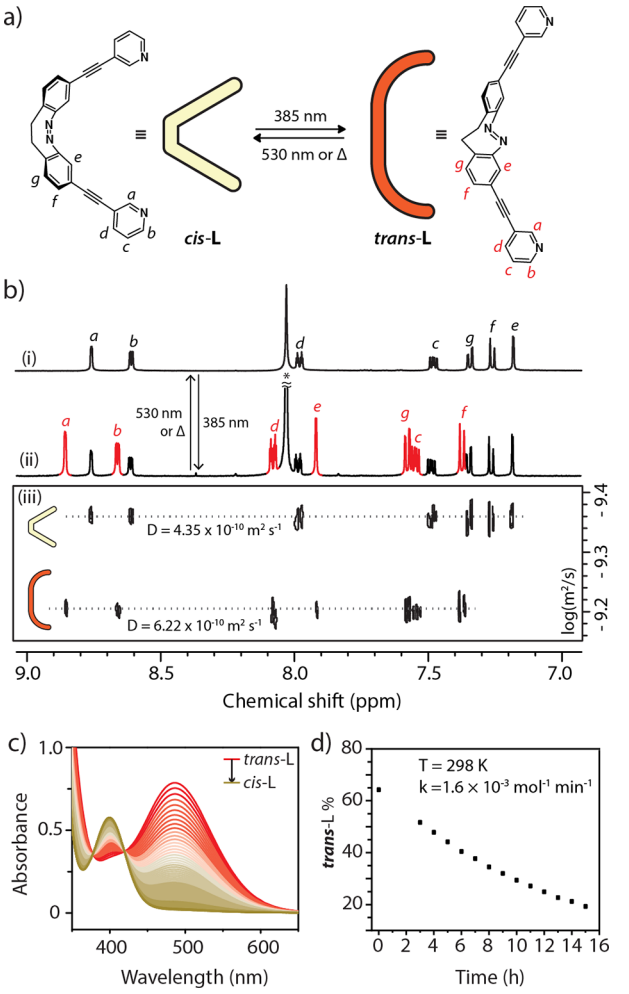

Figure 1. (a) Photoswitching between the two **L** isomers; (b) ^{1}H NMR (500 MHz, DMF-d_7, 298 K) of (i) ***cis*-L** and (ii) the mixture of ***cis*-L** and ***trans*-L** after irradiation at 385 nm for 10 min, (iii) DOSY of the two ligand isomers; (c) absorption spectra showing the thermal relaxation from ***trans*-L** (red line) to ***cis*-L** (beige line) obtained every 30 min (DMF, 1.12 mM, 298 K); (d) kinetics of ***trans*-L** isomerization, monitored by ^{1}H NMR.

Next, we investigated the formation of Pd-based assemblies starting with the stable isomer ***cis*-L**. Reaction of the ligand with $[Pd(CH_3CN)_4](BF_4)_2$ in a 2:1 stoichiometry in DMF as a solvent was investigated by NMR and ESI-MS. Upon addition of Pd^{II}, the ^{1}H NMR signals of ***cis*-L** are significantly broadened, complicating the assignment, while clearly downfield shifted, as typically observed for pyridyl ligands upon Pd coordination (Figure 2b$_{i,ii}$). From geometric considerations, the expected species would be a Pd_2L_4 cage; however, the NMR spectra suggest a more complex scenario, with the presence of multiple species obeying the formula $[Pd_n\textbf{\textit{cis}-L}_{2n}]$ (hereafter named "***cis*-Cage**"). High-resolution ESI-MS analysis supports this hypothesis, showing the formation of species with stoichiometry Pd_2L_4 at m/z = 647.47 ($[Pd_2\textbf{\textit{cis}-L}_4+BF_4]^{3+}$) and Pd_3L_6 at 748.15 ($[Pd_3\textbf{\textit{cis}-L}_6+2BF_4]^{4+}$), while the peaks at 463.10 and 1013.21 consist of an overlap of Pd_2L_4 and Pd_3L_6 species (Figure 2c). Trapped ion mobility spectra (tims) for the peaks corresponding to the empty cages show two collisional cross section (CCS) values, clearly indicating the difference in size between the two species (Figure S38). Formation of a mixture of species with different nuclearity is

https://doi.org/10.1021/jacs.1c12011
J. Am. Chem. Soc. 2022, 144, 3099–3105

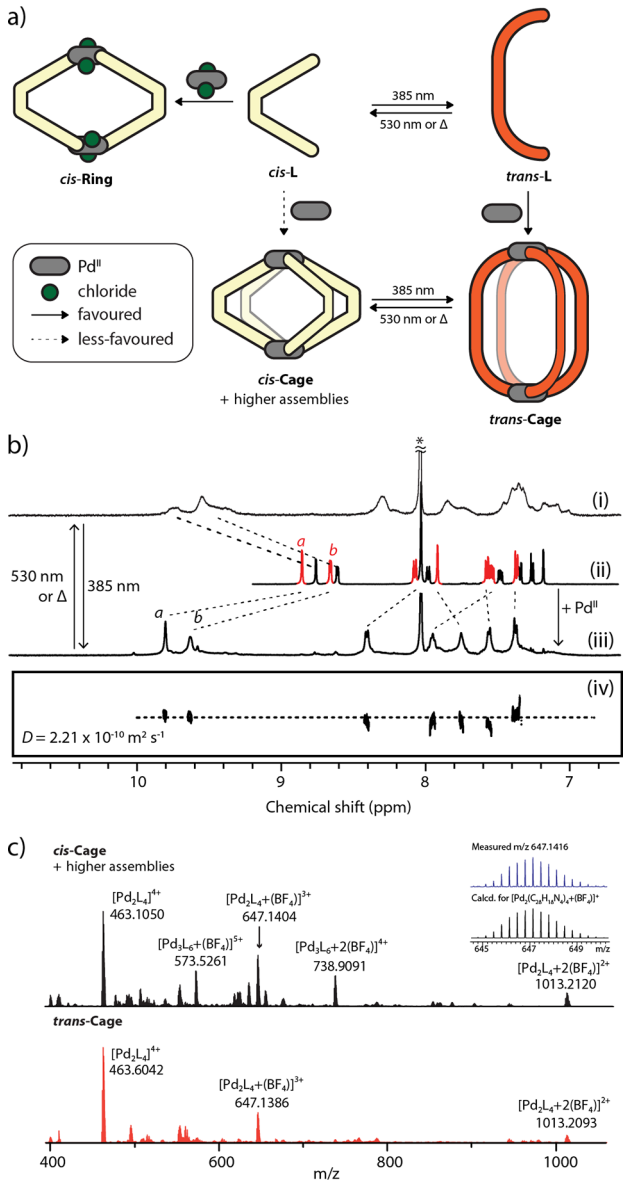

Figure 2. (a) Assembly of ***cis*-Ring**, ***cis*-Cage** (+ higher assemblies), and ***trans*-Cage** and structural interconversion via light or thermal relaxation; (b) ^{1}H NMR spectra (500 MHz, DMF-d_7, 298 K) of (i) ***cis*-L** + $[Pd(CH_3CN)_4](BF_4)_2$ (2:1 mol ratio), (ii) a mixture of ***cis*-L** and ***trans*-L** after 385 nm UV irradiation, (iii) formation of ***trans*-Cage**, (iv) DOSY spectra for ***trans*-Cage**; (c) ESI mass spectra of ***cis*-Cage** (+ higher assemblies; top) and ***trans*-Cage** (bottom).

not uncommon in metallosupramolecular assembly;[44−48] however, the broad NMR spectra suggest the additional formation of larger oligomers, probably undergoing rapid ligand exchange, that are not detectable by ESI-MS. As an explanation for observing such a mixture of ill-defined assembly products, we assumed the accumulation of strain in the assemblies, resulting from a nonideal geometry of the *cis*-isomeric ligand that hampers formation of stable cage- or ring-like three-dimensional structures. In an attempt to release strain from the system, we combined ***cis*-L** with the metal precursor $[PdCl_2(CH_3CN)_2]$ in a 1:1 ratio, indeed resulting in the clean formation of a $[Pd_2Cl_4$***cis*-$L_2]$ (***cis*-Ring**) metallocycle (Figure 2a). Single crystals of the compound were obtained from a DMF/CH_2Cl_2 mixture and subjected to single-crystal X-ray diffraction, delivering a structure in the $P\bar{1}$ space group with half a molecule in the asymmetric unit (Figure 3b). In this

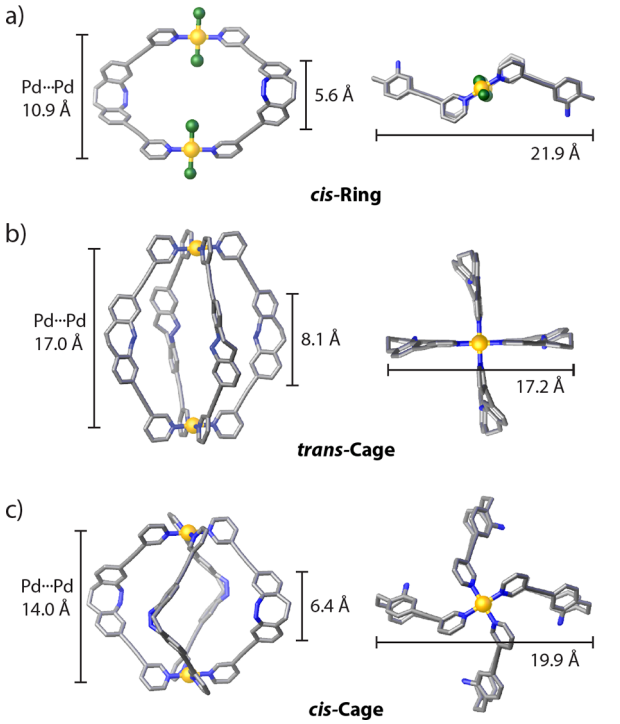

Figure 3. Crystal structures and molecular dimensions of (a) ***cis*-Ring**, (b) ***trans*-Cage**, and (c) DFT-optimized model for $[Pd_2$***cis*-$L_4]$. Short distances on the left side measured between diazocine C_{ipso} atoms; distances on the right, between opposite ethylene bridge carbon atoms.

structure, the two bis-pyridyl ligands, and consequently the coordinated Cl anions, were found to adopt a *trans*-arrangement, hence leaving more space and conformational freedom for the diazocine-based ligands than in the corresponding $[Pd_2$***cis*-$L_4]$ assembly, which is conformationally more constrained owing to its tricyclic topology.

On the other hand, self-assembly of Pd^{II} ions with the meta stable ***trans*-L** in a 1:2 ratio unambiguously results in formation of $[Pd_2$***trans*-$L_4]$ (***trans*-Cage**), as shown by NMR, ESI-MS, and X-ray analysis. ^{1}H NMR spectra show rather sharp signals compared to the ones obtained for the *cis*-system. By addition of an internal standard (1,3,5-tris-*tert*-butylbenzene), we estimated the conversion into ***trans*-Cage** to be about 65% (Figure S14) with respect to the entire ligand content by ^{1}H NMR integration. In line with the values determined for the PSS-governed equilibrium of ligand isomers, this speaks for a quantitative conversion of ***trans*-L** into ***trans*-Cage**. Species of the ***cis*-Cage** mixture are visible as very broad signals below the new set assigned to the ***trans*-Cage**. Overlap with these broad signals prevented a precise determination of the PSS of the assembly mixture. In ***trans*-Cage**, the diagnostic protons H_a and H_b from the pyridine donor groups are downfield shifted from 8.86 to 9.88 ppm and from 8.66 to 9.66 ppm, respectively, confirming coordination to Pd^{II} (Figure 2b$_{iii}$). DOSY analysis corroborates the presence of a single component with r_H = 12.4 Å (Figure 2b$_{vi}$), a value matching with the formation of a $[Pd_2L_4]$ topology. The $[Pd_2L_4]$ stoichiometry was further supported by ESI-MS analysis. A comparison with the data obtained for the assembly products

https://doi.org/10.1021/jacs.1c12011
J. Am. Chem. Soc. 2022, 144, 3099−3105

of ***cis*-L** with Pd^{II} cations clearly showed exclusive formation of $[Pd_2$***trans*-L**$_4]$ and no species with higher nuclearity (Figure 2c). Ultimate confirmation for the formation of a dinuclear cage was provided by single-crystal X-ray crystallography. Single crystals of $[Pd_2$***trans*-L**$_4]$ were obtained by vapor diffusion of diethyl ether into a DMF solution of the cage at 4 °C in the absence of light (Figure 3a). Low temperature and dark conditions were essential for successful crystal growth and measurement in order to isolate the compound with all diazocine photoswitches residing in the metastable *trans*-isomeric state. $[Pd_2$***trans*-L**$_4]$ crystallizes in a triclinic $P\bar{1}$ space group, revealing a C_2-symmetry with respect to the relative conformation of the eight-membered rings. The Pd···Pd distance was measured as 17.0 Å, significantly longer than that found in the ***cis*-Ring** (10.9 Å), the latter showing a more folded conformation. To the best of our knowledge, only two examples of crystal structures for a *trans*-diazocine have been reported so far,[49,50] none of them carrying any substituents.

As no X-ray structure could be obtained for the $[Pd_2$***cis*-L**$_4]$ species, a gas-phase structure for this cage photoisomer was determined by density functional theory (DFT) geometry optimization (for details see the Supporting Information). When comparing the calculated $[Pd_2$***cis*-L**$_4]$ ***cis*-Cage** structure with the X-ray result of ***cis*-Ring**, it caught our attention that the *cis*-diazocine moiety is significantly stretched in the former structure (C_{ipso}–C_{ipso} distance = 6.4 Å; Figure 3c) as compared to the latter (5.6 Å; corresponding distance in the DFT geometry-optimized ring: 5.7 Å; X-ray of free *cis*-diazocine: 5.9 Å[41]), and a similar observation was made when comparing the Pd–Pd distances (Figure 3b and c). Apparently, the assembly of ***cis*-L** to $[Pd_2$***cis*-L**$_4]$ would force the diazocines to stretch to an unfavorable extent. This energetic disadvantage drives the system towards the formation of an ill-defined mixture of species with different nuclearities showing highly dynamic ligand exchange.

Furthermore, a plausible explanation for the clean formation of a $[Pd_2$***trans*-L**$_4]$ species, in contrast to the ***cis*-Cage** situation, could be obtained by comparing energies derived from DFT calculations. Therefore, the strain energies of the structures of $[Pd_2$***cis*-L**$_4]$, ***trans*-Cage**, and ***cis*-Ring** were compared by computing energies for ligand and coordination site fragments in their assembly-derived and relaxed conformations, respectively. Results of the calculations show that formation of the tentative $[Pd_2$***cis*-L**$_4]$ (Figure 3c) species suffers from significant strain compared to the sterically less congested and conformationally more flexible ***cis*-Ring**, as well as compared to the ***trans*-Cage** (see the Supporting Information for details). These results support that formation of the experimentally observed ***trans*-Cage** is favored, even if it persists only in a transient state under continuous irradiation with UV light to prevent thermal back-transformation.

Interestingly, the photoswitching properties of the ligand were maintained in the cage structure. Upon irradiation of the ***cis*-Cage** mixture with a 385 nm LED for 10 min, the sample converts into the ***trans*-Cage**. Again, the process is reversible, and irradiation at λ = 530 nm or thermal relaxation restore the ***cis*-Cage** mixture, as clearly shown by ^{1}H NMR analysis (Figures 2b, S13). UV–vis analysis results of the cage species are similar to those of the ligands, with an absorption band centered at 395 nm for ***cis*-Cage** and an increasing band at 483 nm for ***trans*-Cage** upon irradiation at λ = 385 nm (Figure 4a). The photoswitching is reversible and shows no significant fatigue over numerous cycles (Figure 4b). The thermal

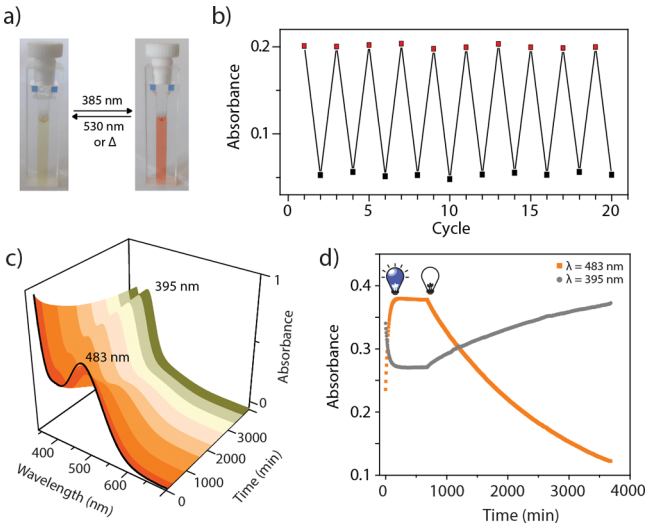

Figure 4. (a) Cage solution color change after irradiation (pale yellow: ***cis*-Cage** (+ higher assemblies), red: ***trans*-Cage**); (b) fatigue experiment of structural interconversion upon irradiation with 385 and 530 nm in an alternating sequence; absorbance values measured at λ = 483 nm; (c) time-dependent UV–vis spectra showing thermal relaxation from the ***trans*-Cage** to ***cis*-Cage** mixture; (d) UV–vis monitoring of the system reaching the PSS and maintaining the out-of-equilibrium state (***trans*-Cage**) with constant irradiation at 385 nm; turning off the light leads to thermal decay.

relaxation follows a first-order kinetics, and rate constant k and half-lifetime $t_{1/2}$ of the ***trans*-Cage** were determined (Supporting Information). The half-life for the supramolecular cage ($t_{1/2}$ = 6.1 h) at 298 K is comparable, while slightly shorter, to that of ***trans*-L** ($t_{1/2}$ = 7.2 h) at the same temperature. Temperature-dependent kinetic studies were carried out for both cage and ligand to determine the activation parameters using the Eyring–Polanyi equation, as reported in Table 1. The results clearly show how the ligand's photoswitching properties are maintained upon formation of the supramolecular cage.

Table 1. Activation Energies for *Trans* to *Cis* Isomerization

	$\Delta S^{\ddagger}$ (J/mol K)	$\Delta H^{\ddagger}$ (kJ/mol)	$\Delta G^{\ddagger}$ (kJ/mol) at 298 K
***trans*-C to *cis*-C**	30.7	97.3	88.1
***trans*-L to *cis*-L**	24.2	96.2	89.0

As detailed above, ***trans*-Cage** is accessible only when energy, in the form of light, is provided to the system. To prove this, we monitored the UV–vis spectrum of the system under constant irradiation at a fixed temperature, using a home-built setup. Irradiation of the ***cis*-Cage** at λ = 385 nm was performed with a 90° incidence angle with respect to the direction of the source and detector of the spectrophotometer, equipped with a thermostat to keep the sample at 288 K. The diagnostic absorption bands at 395 and 483 nm reveal that upon irradiation, the ***cis*-Cage** system rapidly converts into ***trans*-Cage**, and upon reaching the PSS, the ratio of *cis*- and *trans*-isomers is kept constant while the light stimulus is continuously applied. Upon removal of the light source, the transient state of the system dominated by the ***trans*-Cage** immediately starts transforming into the ***cis*-Cage** system by thermal relaxation (Figure 4c,d).

https://doi.org/10.1021/jacs.1c12011
J. Am. Chem. Soc. 2022, 144, 3099–3105

Finally, we investigated the host–guest properties of both *cis*- and *trans*-systems with bis-anionic guest 2,6-naphthalene bissulfonate (**G**) (Figure 5a). NMR titration of the ***cis*-Cage**

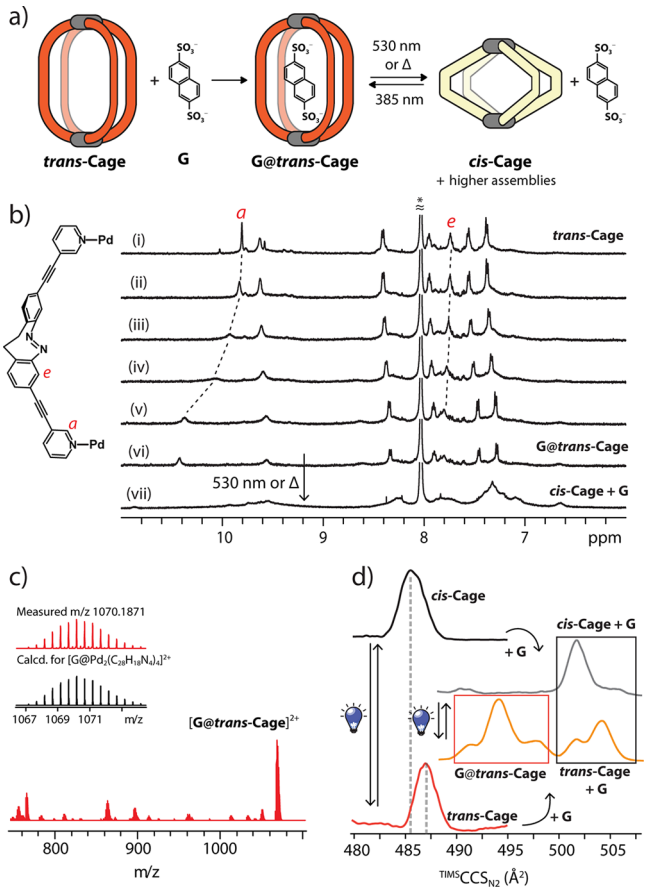

Figure 5. (a) Guest uptake of ***trans*-Cage** and release by isomerization to ***cis*-Cage**; (b) ^{1}H NMR (500 MHz, DMF-d_7, 298 K) stepwise addition of guest **G** to ***trans*-Cage** (mole ratio of host:guest = (i) 1:0.2, (ii) 1:0.4, (iii) 1:0.6, (iv) 1:0.8, and (v) 1:1.0) followed by photoswitching (vii); (c) ESI-MS of **G@*trans*-Cage**; (d) ion mobility spectra for ***cis*-Cage**, ***cis*-Cage+G**, ***trans*-Cage**, and **G@*trans*-Cage** and light-induced reversibility of the process. The red box highlights signals for inside binding; the black box, signals for outside binding.

mixture with **G** resulted in even further broadening of the signals, accompanied by decreasing intensity and onset of precipitation after the addition of 0.3 equiv of guest, indicative of an outside association mode, creating a salt of low solubility (Figure S35).[51,52] On the contrary, ***trans*-Cage** is clearly able to bind the guest molecule in its cavity, in accordance with previously reported hosts for **G** showing a comparable cavity size.[52] According to ^{1}H NMR spectroscopy, stepwise addition of **G** into the cage solution results in a gradual downfield shift of the inward-pointing protons H_e and H_a, evidencing encapsulation (Figure 5b). Unfortunately, it was not possible to determine the association constant due to an onset of precipitation after the addition of 1 guest equivalent. The host–guest behavior was investigated also by trapped ion mobility spectrometry coupled to ESI-TOF-MS (timsTOF). Here, it was possible to detect signals indicative of an interaction of **G** with both ***cis*-** and ***trans*-Cage** (Figures 5c, S31). In the case of the *cis*-isomer, however, the main species are the "empty" assembly $[Pd_2$***cis*-**$L_4]^{4+}$ at m/z = 463.10, as well as compounds with stoichiometry $[Pd_3$***cis*-**$L_5G]^{4+}$ at m/z = 664.36, $[Pd_4$***cis*-**$L_6G_2]^{4+}$ at m/z = 865.11, and $[Pd_4$***cis*-**$L_7G_2]^{4+}$ at m/z = 967.90, where presumably the guest replaces one or more ligands (or ligand arms) in coordinated positions in order to reduce strain. Species $[Pd_2$***cis*-**L_4+**G**$]^{2+}$, corresponding to a typical 1:1 host:guest complex stoichiometry at m/z = 1070.19, was only detected as a minor component (Figure S36). On the contrary, the mass spectrum of the *trans*-isomeric host in the presence of **G** features the signal at m/z = 1070.19 assigned to $[$**G**$@Pd_2$***trans*-**$L_4]^{2+}$ as the predominant species (Figure 5c). In order to further investigate whether the guest binds inside or interacts with the outside of the cages, we performed an ion mobility analysis focusing on the 2+ peaks assigned to the $[Pd_2L_4+2BF_4]^{2+}$ and $[Pd_2L_4+$**G**$]^{2+}$ species for both the *cis*- and *trans*-isomers. Addition of **G** to the ***trans*-Cage** shows two CCSs, corresponding to larger objects (494.1 and 504.4 Å^2) as compared to the "empty" host (487.4 Å^2) and assigned to *inside* and *outside* guest binding modes, respectively (Figure 5d). Analysis of the small MS peak at m/z = 1070.19 for $[Pd_2$***cis*-**L_4+**G**$]^{2+}$ shows only one CCS value of 501.7 Å^2, comparable to the *outside* guest binding mode observed for ***trans*-Cage**, hence further supporting that the guest cannot enter the cavity of $[Pd_2$***cis*-**$L_4]$ but rather associates nonspecifically to the cage's exterior (Figure 5d).

Furthermore, guest binding and release was found to be reversible upon application of the light stimulus. Irradiation (λ = 385 nm) of the system to the metastable ***trans*-Cage** leads to guest binding, while reversing the photoswitching (λ = 530 nm or Δ) leads to guest release, as determined by stepwise irradiation combined with ion mobility experiments (Figure 5d, Figure S40). Noteworthy, formation of $[$**G**$@Pd_2$***trans*-**$L_4]^{2+}$ represents an example of dissipative self-assembly, since this state is existing only under continuous irradiation. Removal of the light stimulus fueling maintenance of this complex leads to thermal relaxation of the diazocine moiety to the *cis*-form, disassembly of the host, and consequently guest release.

■ CONCLUSIONS

In conclusion, we reported the first coordination-driven cage embedding a diazocine photoswitch.[53] The photophysical properties of the diazocine moiety are maintained in the supramolecular assembly, and the system can reversibly switch between a ***cis*-** and ***trans*-Cage** system. The thermodynamically more stable ligand isomer ***cis*-L** leads to an ill-defined mixture of $[Pd_n$***cis*-**$L_{2n}]_n$ (n = 2, 3, ...) compounds as a consequence of an unfavorable ligand conformation. Strain in this system can be released when assembling a ring topology, as shown by the crystal structure of a $[Pd_2Cl_4$***cis*-**$L_2]$ ring and DFT calculations. Metastable ***trans*-L** self-assembles with Pd^{II} to a $[Pd_2L_4]$ cage as exclusive product, as confirmed by NMR, MS, and single-crystal X-ray results. However, $[Pd_2$***trans*-**$L_4]$ is maintained only under continuous irradiation with UV light, and removal of the stimulus results in thermal relaxation to re-form the ***cis*-Cage** system. Only the metastable ***trans*-Cage** is able to bind a guest molecule. The host–guest system is thus formed *via* dissipative self-assembly and exists only under constant input of energy in the form of light. Upon reversal of ligand isomerization, by irradiation at 530 nm or thermal back-switching, ***trans*-Cage** disassembles and releases the guest. The herein introduced building blocks and principles offer potential for controlling functions in molecular machinery, generating stimuli-responsive complex systems and models for autopoietic processes.

https://doi.org/10.1021/jacs.1c12011
J. Am. Chem. Soc. 2022, 144, 3099–3105

■ ASSOCIATED CONTENT

Supporting Information

The Supporting Information is available free of charge at https://pubs.acs.org/doi/10.1021/jacs.1c12011.

Synthetic procedures, NMR, MS, UV−vis spectroscopic data, SCXRD results, and DFT calculation data (PDF)

Accession Codes

CCDC 2117884−2117885 contain the supplementary crystallographic data for this paper. These data can be obtained free of charge via www.ccdc.cam.ac.uk/data_request/cif, or by emailing data_request@ccdc.cam.ac.uk, or by contacting The Cambridge Crystallographic Data Centre, 12 Union Road, Cambridge CB2 1EZ, UK; fax: +44 1223 336033.

■ AUTHOR INFORMATION

Corresponding Author

Guido H. Clever − *Department of Chemistry and Chemical Biology, TU Dortmund University, 44227 Dortmund, Germany;* orcid.org/0000-0001-8458-3060; Email: guido.clever@tu-dortmund.de

Authors

Haeri Lee − *Department of Chemistry and Chemical Biology, TU Dortmund University, 44227 Dortmund, Germany; Department of Chemistry, Hannam University, Daejeon 34054, Republic of Korea*

Jacopo Tessarolo − *Department of Chemistry and Chemical Biology, TU Dortmund University, 44227 Dortmund, Germany*

Daniel Langbehn − *Otto Diels Institute of Organic Chemistry, Christian-Albrechts University, 24118 Kiel, Germany*

Ananya Baksi − *Department of Chemistry and Chemical Biology, TU Dortmund University, 44227 Dortmund, Germany*

Rainer Herges − *Otto Diels Institute of Organic Chemistry, Christian-Albrechts University, 24118 Kiel, Germany;* orcid.org/0000-0002-6396-6991

Complete contact information is available at: https://pubs.acs.org/10.1021/jacs.1c12011

Author Contributions

The manuscript was written through contributions of all authors.

Notes

The authors declare no competing financial interest.

■ ACKNOWLEDGMENTS

This work was supported by the European Research Council (ERC Consolidator grant 683083, RAMSES). H.L. thanks the National Research Foundation of Korea (grant NRF-2021R1C1C1013037). R.H. and D.L. are grateful for support by the DFG via SFB 677.

■ REFERENCES

(1) Saha, S.; Regeni, I.; Clever, G. H. Structure Relationships between Bis-Monodentate Ligands and Coordination Driven Self-Assemblies. *Coord. Chem. Rev.* **2018**, *374*, 1−14.

(2) Pullen, S.; Tessarolo, J.; Clever, G. H. Increasing Structural and Functional Complexity in Self-Assembled Coordination Cages. *Chem. Sci.* **2021**, *12*, 7269−72393.

(3) Chakrabarty, R.; Mukherjee, P. S.; Stang, P. J. Supramolecular Coordination: Self-Assembly of Finite Two- and Three-Dimensional Ensembles. *Chem. Rev.* **2011**, *111*, 6810−6918.

(4) Ward, M. D.; Hunter, C. A.; Williams, N. H. Coordination Cages Based on Bis(Pyrazolylpyridine) Ligands: Structures, Dynamic Behavior, Guest Binding, and Catalysis. *Acc. Chem. Res.* **2018**, *51*, 2073−2082.

(5) Davis, A. V.; Fiedler, D.; Seeber, G.; Zahl, A.; van Eldik, R.; Raymond, K. N. Guest Exchange Dynamics in an M4L6 Tetrahedral Host. *J. Am. Chem. Soc.* **2006**, *128*, 1324−1333.

(6) Löffler, S.; Wuttke, A.; Zhang, B.; Holstein, J. J.; Mata, R. A.; Clever, G. H. Influence of Size, Shape, Heteroatom Content and Dispersive Contributions on Guest Binding in a Coordination Cage. *Chem. Commun.* **2017**, *53*, 11933−11936.

(7) August, D. P.; Nichol, G. S.; Lusby, P. J. Maximizing Coordination Capsule−Guest Polar Interactions in Apolar Solvents Reveals Significant Binding. *Angew. Chem., Int. Ed.* **2016**, *55*, 15022−15026.

(8) Li, R.-J.; Holstein, J. J.; Hiller, W. G.; Andréasson, J.; Clever, G. H. Mechanistic Interplay between Light Switching and Guest Binding in Photochromic [Pd2Dithienylethene4] Coordination Cages. *J. Am. Chem. Soc.* **2019**, *141*, 2097−2103.

(9) Castilla, A. M.; Ronson, T. K.; Nitschke, J. R. Sequence-Dependent Guest Release Triggered by Orthogonal Chemical Signals. *J. Am. Chem. Soc.* **2016**, *138*, 2342−2351.

(10) Li, R.-J.; Tessarolo, J.; Lee, H.; Clever, G. H. Multi-Stimuli Control over Assembly and Guest Binding in Metallo-Supramolecular Hosts Based on Dithienylethene Photoswitches. *J. Am. Chem. Soc.* **2021**, *143*, 3865−3873.

(11) Rizzuto, F. J.; von Krbek, L. K. S.; Nitschke, J. R. Strategies for Binding Multiple Guests in Metal−Organic Cages. *Nat. Rev. Chem.* **2019**, *3*, 204−222.

(12) Kim, T. Y.; Vasdev, R. A. S.; Preston, D.; Crowley, J. D. Strategies for Reversible Guest Uptake and Release from Metallosupramolecular Architectures. *Chem.—Eur. J.* **2018**, *24*, 14878−14890.

(13) Jansze, S. M.; Cecot, G.; Severin, K. Reversible Disassembly of Metallasupramolecular Structures Mediated by a Metastable-State Photoacid. *Chem. Sci.* **2018**, *9*, 4253−4257.

(14) Xu, L.; Zhang, D.; Ronson, T. K.; Nitschke, J. R. Improved Acid Resistance of a Metal−Organic Cage Enables Cargo Release and Exchange between Hosts. *Angew. Chem., Int. Ed.* **2020**, *59*, 7435−7438.

(15) Jansze, S. M.; Severin, K. Palladium-Based Metal−Ligand Assemblies: The Contrasting Behavior upon Addition of Pyridine or Acid. *J. Am. Chem. Soc.* **2019**, *141*, 815−819.

(16) Zhang, D.; Ronson, T. K.; Güryel, S.; Thoburn, J. D.; Wales, D. J.; Nitschke, J. R. Temperature Controls Guest Uptake and Release from Zn 4 L 4 Tetrahedra. *J. Am. Chem. Soc.* **2019**, *141*, 14534−14538.

(17) Cai, L.-X.; Yan, D.-N.; Cheng, P.-M.; Xuan, J.-J.; Li, S.-C.; Zhou, L.-P.; Tian, C.-B.; Sun, Q.-F. Controlled Self-Assembly and Multistimuli-Responsive Interconversions of Three Conjoined Twin-Cages. *J. Am. Chem. Soc.* **2021**, *143*, 2016−2024.

(18) Szalóki, G.; Croué, V.; Carré, V.; Aubriet, F.; Alévêque, O.; Levillain, E.; Allain, M.; Aragó, J.; Ortí, E.; Goeb, S.; Sallé, M. Controlling the Host−Guest Interaction Mode through a Redox Stimulus. *Angew. Chem., Int. Ed.* **2017**, *56*, 16272−16276.

(19) Croué, V.; Goeb, S.; Szalóki, G.; Allain, M.; Sallé, M. Reversible Guest Uptake/Release by Redox-Controlled Assembly/Disassembly of a Coordination Cage. *Angew. Chem., Int. Ed.* **2016**, *55*, 1746−1750.

(20) Preston, D.; Fox-Charles, A.; Lo, W. K. C.; Crowley, J. D. Chloride Triggered Reversible Switching from a Metallosupramolecular [Pd2L4]4+ Cage to a [Pd2L2Cl4] Metallo-Macrocycle with Release of Endo - and Exo -Hedrally Bound Guests. *Chem. Commun.* **2015**, *51*, 9042−9045.

(21) Zhu, R.; Lübben, J.; Dittrich, B.; Clever, G. H. Stepwise Halide-Triggered Double and Triple Catenation of Self-Assembled Coordination Cages. *Angew. Chem., Int. Ed.* **2015**, *54*, 2796−2800.

(22) Bandara, H. M. D.; Burdette, S. C. Photoisomerization in Different Classes of Azobenzene. *Chem. Soc. Rev.* **2012**, *41*, 1809−1825.
(23) Oshchepkov, A. S.; Namashivaya, S. S. R.; Khrustalev, V. N.; Hampel, F.; Laikov, D. N.; Kataev, E. A. Control of Photoisomerization of an Azoazacryptand by Anion Binding and Cucurbit[8]Uril Encapsula-tion in an Aqueous Solution. *J. Org. Chem.* **2020**, *85*, 9255−9263.
(24) Tian, H.; Yang, S. Recent Progresses on Diarylethene Based Photochromic Switches. *Chem. Soc. Rev.* **2004**, *33*, 85−97.
(25) Qin, Y.; Wang, Y.-T.; Yang, H.-B.; Zhu, W. Recent Advances on the Construction of Diarylethene-Based Supramolecular Metallacycles and Metallacages via Coordination-Driven Self-Assembly. *Chem. Synth.* **2021**, *1:2*.
(26) Koumura, N.; Zijlstra, R. W. J.; van Delden, R. A.; Harada, N.; Feringa, B. L. Light-Driven Monodirectional Molecular Rotor. *Nature* **1999**, *401*, 152−155.
(27) Ruangsupapichat, N.; Pollard, M. M.; Harutyunyan, S. R.; Feringa, B. L. Reversing the Direction in a Light-Driven Rotary Molecular Motor. *Nat. Chem.* **2011**, *3*, 53−60.
(28) Petermayer, C.; Dube, H. Indigoid Photoswitches: Visible Light Responsive Molecular Tools. *Acc. Chem. Res.* **2018**, *51*, 1153−1163.
(29) Berton, C.; Busiello, D. M.; Zamuner, S.; Scopelliti, R.; Fadaei-Tirani, F.; Severin, K.; Pezzato, C. Light-Switchable Buffers. *Angew. Chem., Int. Ed.* **2021**, *60*, 21737−21740.
(30) Berton, C.; Busiello, D. M.; Zamuner, S.; Solari, E.; Scopelliti, R.; Fadaei-Tirani, F.; Severin, K.; Pezzato, C. Thermodynamics and Kinetics of Protonated Merocyanine Photoacids in Water. *Chem. Sci.* **2020**, *11*, 8457−8468.
(31) Ragazzon, G.; Prins, L. J. Energy Consumption in Chemical Fuel-Driven Self-Assembly. *Nat. Nanotechnol.* **2018**, *13*, 882−889.
(32) Ragazzon, G.; Baroncini, M.; Silvi, S.; Venturi, M.; Credi, A. Light-Powered Autonomous and Directional Molecular Motion of a Dissipative Self-Assembling System. *Nat. Nanotechnol.* **2015**, *10*, 70−75.
(33) Stuckhardt, C.; Roke, D.; Danowski, W.; Otten, E.; Wezenberg, S. J.; Feringa, B. L. A Chiral Self-Sorting Photoresponsive Coordination Cage Based on Overcrowded Alkenes. *Beilstein J. Org. Chem.* **2019**, *15*, 2767−2773.
(34) Fu, S.; Luo, Q.; Zang, M.; Tian, J.; Zhang, Z.; Zeng, M.; Ji, Y.; Xu, J.; Liu, J. Light-Triggered Reversible Disassembly of Stimuli-Responsive Coordination Metallosupramolecular Pd2L4 Cages Mediated by Azobenzene-Containing Ligands. *Mater. Chem. Front.* **2019**, *3*, 1238−1243.
(35) Oldknow, S.; Martir, D. R.; Pritchard, V. E.; Blitz, M. A.; Fishwick, C. W. G.; Zysman-Colman, E.; Hardie, M. J. Structure-Switching M3L2Ir(III) Coordination Cages with Photo-Isomerising Azo-Aromatic Linkers. *Chem. Sci.* **2018**, *9*, 8150−8159.
(36) Han, M.; Luo, Y.; Damaschke, B.; Gómez, L.; Ribas, X.; Jose, A.; Peretzki, P.; Seibt, M.; Clever, G. H. Light-Controlled Interconversion between a Self-Assembled Triangle and a Rhombicuboctahedral Sphere. *Angew. Chem., Int. Ed.* **2016**, *55*, 445−449.
(37) Li, R.; Han, M.; Tessarolo, J.; Holstein, J. J.; Lübben, J.; Dittrich, B.; Volkmann, C.; Finze, M.; Jenne, C.; Clever, G. H. Successive Photoswitching and Derivatization Effects in Photochromic Dithienylethene-Based Coordination Cages. *Chemphotochem* **2019**, *3*, 378−383.
(38) Gu, Y.; Alt, E. A.; Wang, H.; Li, X.; Willard, A. P.; Johnson, J. A. Photoswitching Topology in Polymer Networks with Metal−Organic Cages as Crosslinks. *Nature* **2018**, *560*, 65−69.
(39) Zhang, Y.; Zhou, Y.; Gao, T.; Yan, P.; Li, H. Metal-Directed Synthesis of Quadruple-Stranded Helical Eu(III) Molecular Switch: A Significant Improvement in Photocyclization Quantum Yield. *Chem. Commun.* **2020**, *56*, 13213−13216.
(40) Li, M.; Chen, L.-J.; Zhang, Z.; Luo, Q.; Yang, H.-B.; Tian, H.; Zhu, W.-H. Conformer-Dependent Self-Assembled Metallacycles with Photo-Reversible Response. *Chem. Sci.* **2019**, *10*, 4896−4904.
(41) Siewertsen, R.; Neumann, H.; Buchheim-Stehn, B.; Herges, R.; Näther, C.; Renth, F.; Temps, F. Highly Efficient Reversible Z−E Photoisomerization of a Bridged Azobenzene with Visible Light through Resolved S1(Nπ*) Absorption Bands. *J. Am. Chem. Soc.* **2009**, *131*, 15594−15595.
(42) Moormann, W.; Langbehn, D.; Herges, R. Synthesis of Functionalized Diazocines for Application as Building Blocks in Photo- and Mechanoresponsive Materials. *Beilstein J. Org. Chem.* **2019**, *15*, 727−732.
(43) Moormann, W.; Tellkamp, T.; Stadler, E.; Röhricht, F.; Näther, C.; Puttreddy, R.; Rissanen, K.; Gescheidt, G.; Herges, R. Efficient Conversion of Light to Chemical Energy: Directional, Chiral Photoswitches with Very High Quantum Yields. *Angew. Chem., Int. Ed.* **2020**, *59*, 15081−15086.
(44) Tessarolo, J.; Lee, H.; Sakuda, E.; Umakoshi, K.; Clever, G. H. Integrative Assembly of Heteroleptic Tetrahedra Controlled by Backbone Steric Bulk. *J. Am. Chem. Soc.* **2021**, *143*, 6339−6344.
(45) Zhang, T.; Zhou, L.-P.; Guo, X.-Q.; Cai, L.-X.; Sun, Q.-F. Adaptive Self-Assembly and Induced-Fit Transformations of Anion-Binding Metal-Organic Macrocycles. *Nat. Commun.* **2017**, *8*, 15898.
(46) Chand, D. K.; Biradha, K.; Kawano, M.; Sakamoto, S.; Yamaguchi, K.; Fujita, M. Dynamic Self-Assembly of an M3L6Molecular Triangle and an M4L8 Tetrahedron from Naked PdII Ions and Bis(3-pyridyl)-Substituted Arenes. *Chem.—Asian J.* **2006**, *1*, 82−90.
(47) Rancan, M.; Tessarolo, J.; Zanonato, P. L.; Seraglia, R.; Quici, S.; Armelao, L. Self-Assembly of a Constitutional Dynamic Library of Cu(II) Coordination Polygons and Reversible Sorting by Crystallization. *Dalton Trans.* **2013**, *42*, 7534−7538.
(48) Hasenknopf, B.; Lehn, J.-M.; Boumediene, N.; Dupont-Gervais, A.; Van Dorsselaer, A.; Kneisel, B.; Fenske, D. Self-Assembly of Tetra- and Hexanuclear Circular Helicates. *J. Am. Chem. Soc.* **1997**, *119*, 10956−10962.
(49) Jun, M.; Joshi, D. K.; Yalagala, R. S.; Vanloon, J.; Simionescu, R.; Lough, A. J.; Gordon, H. L.; Yan, H. Confirmation of the Structure of Trans-Cyclic Azobenzene by X-Ray Crystallography and Spectroscopic Characterization of Cyclic Azobenzene Analogs. *Chem.* **2018**, *3*, 2697−2701.
(50) Krämer, R.; Nöthling, N.; Lehmann, C. W.; Mohr, F.; Tausch, M. W. E-Diazocine in Chemical Education: Synthesis, Structure, Photochromism and Thermal Stability. *Chemphotochem* **2018**, *2*, 6−11.
(51) Clever, G. H.; Tashiro, S.; Shionoya, M. Light-Triggered Crystallization of a Molecular Host−Guest Complex. *J. Am. Chem. Soc.* **2010**, *132*, 9973−9975.
(52) Clever, G. H.; Kawamura, W.; Shionoya, M. Encapsulation versus Aggregation of Metal−Organic Cages Controlled by Guest Size Variation. *Inorg. Chem.* **2011**, *50*, 4689−4691.
(53) For a recent example of cages based on ligands with an azobenzene backbone see: Cecot, P.; Walczak, A.; Markiewicz, G.; Stefankiewicz, A. R. Gating the photoactivity of azobenzene-type ligands trapped within a dynamic system of an M4L6 tetrahedral cage, an M2L2 metallocycle and mononuclear MLn complexes. *Inorg. Chem. Front.* **2021**, *8*, 5195−5200.

https://doi.org/10.1021/jacs.1c12011
J. Am. Chem. Soc. 2022, 144, 3099−3105